Ferromagnetically coupled single-chain magnets exhibiting a magnetic hysteresis of 0.42 Tesla in cyano-bridged $Fe^{III}_2M^{II}$ (M = Ni, Fe) coordination polymers

Jin-Hua Wang[a,b], Mohammad Khurram Javed[a], Jia-Xin Li[c], Yi-Quan Zhang[c], Zhao-Yang Li[a], and Masahiro Yamashita[d]*

[a]*School of Materials Science and Engineering, Nankai University, 38 Tongyan Road, Tianjin 300350, P. R. China*

[b]*Shandong Provincial Engineering Laboratory of Novel Pharmaceutical Excipients, Sustained and Controlled Release Preparations, College of Medicine and Nursing, Dezhou University, Dezhou 253023, P. R. China*

[c]*School of Physical Science and Technology, Nanjing Normal University, No.1 Wenyuan Road, Qixia District, Nanjing 210023, P. R. China*

[d]*Department of Chemistry, Graduate School of Science, Tohoku University, 6-3 Aramaki-Aza-Aoba, Aoba-ku, Sendai 980-8578, Japan*

Table of Contents

I. General method

1. Materials and methods

The salt $(NEt_4)[Fe^{III}(Tp^*)(CN)_3]$ was prepared according to modified literature method,[1] and other reagents and solvents used were commercially available and not further purified. Thermogravimetric analysis (TGA) was carried out on a Rigaku standard TG-DTA analyzer from room temperature to 700 °C under argon atmosphere with a heating rate of 10 °C min^{-1}, using an empty Pt crucible as reference. Elemental analysis (C, H, and N) was performed on a vario EL cube elemental analyzer. Powder X-ray diffraction (PXRD) was performed on a Rigaku Miniflex 600 at room temperature.

2. X-ray crystallography

Single-crystal X-ray diffraction study were performed on a Rigaku diffractometer equipped with CCD area detector with a graphite monochromator. The determination of unit cell parameters and data collections were performed with Cu-Kα radiation (λ = 1.54 Å). The data were corrected by semi-empirical method using SADABS program. The program SAINT was used for integration of the diffraction profiles. The structure was solved by direct methods using SHELXS program of the SHELXTL-97 package and refined with SHELXL.[2] The final refinements were performed by full matrix least-squares methods with anisotropic thermal parameters for non-hydrogen atoms on F^2. The uncoordinated solvent molecules are disordered, which are removed by SQUEEZE in PLATON,[3] and the results were appended in the CIF file. Finally, a summary of the crystallographic data and structure refinements are listed in Table 1 for **1** and **2**. Selected bond lengths and angles are given in Table S1 and S2.

3. Magnetic measurements

Direct current magnetic susceptibility measurements of polycrystalline samples **1** and **2**, on a Quantum Design SQUID magnetometer, operating between 1.8 and 300 K. alternating current magnetic susceptibility data measurements were performed at frequencies between 1 and 1000 Hz. Data were corrected for the diamagnetic contribution calculated from Pascal's constants.

4. Computational studies

As the prediction and control of the magnetic anisotropy have become crucial for the design of magnetic materials, such as SCMs. In the present study, the mononuclear LS *fac*-[Fe^{III}(Tp*)(CN)$_3$]$^-$ may display a significant magnetic anisotropy, owing to the *ab initio* calculations of the isostructural LS *fac*-[Fe^{III}(Tp)(CN)$_3$]$^-$ with similar C_3 symmetry.[4] To obtain the isotropic exchange coupling constants J between Ni^{II} and Fe^{III}, Orca 4.1.2 calculations[5] were performed with the popular hybrid functional B3LYP proposed by Becke[6] and Lee et al.[7] Triple-ζ with one polarization function TZVP[8] basis sets were used for all atoms, and zero order regular approximation (ZORA) was used for the scalar relativistic effect in all calculations. Four Ni^{II}-Fe^{III} isotropic exchange couplings in the model structure exhibited in Fig. S15 are the same, and thus there is only one type of J between Ni^{II} and Fe^{III}. The large integration grid (grid = 5) was applied to Ni^{II} and Fe^{III} for ZORA calculations. Tight convergence criteria was selected to ensure the results to be well converged with respect to technical parameters.

Complete active space second-order perturbation theory (CASPT2) considering the effect of the dynamical electronic correlation based on complete-active-space self-consistent field (CASSCF) using MOLCAS 8.4 program package[9] was performed on the model structure of individual Ni^{II} fragment (see Fig. S16) extracted from complex **1**. For the first CASSCF calculation, the basis sets for all atoms are atomic natural orbitals from the MOLCAS ANO-RCC library: ANO-RCC-VTZP for magnetic center ion Ni^{II}; VTZ for close N atoms; VDZ for distant atoms. The calculations employed the second order Douglas-Kroll-Hess Hamiltonian, where scalar relativistic contractions were taken into account in the basis set. The effect of the dynamical electronic correlation was applied using CASPT2 based on the first CASSCF calculation. After that, the spin-orbit coupling was handled separately in the restricted active space state interaction (RASSI-SO) procedure. The active electrons in 10 active spaces considering 3d double shell effect include all seven 3d electrons, and the mixed spin-free states are 25 (via 10 quadruplets and 15 doublets).

II. X-ray structure determination

Table S1 Selected bond lengths (Å) and bond angles (°) for **1**.

Fe1–N3	1.989(7)	Fe1–N6	2.006(4)
Fe1–C1	1.904(5)	Fe1–C2	1.934(18)
Ni2–N1	2.067(3)	Ni2–N7	2.096(5)
N1–Ni2–N7	89.28(8)	N1–Ni2–N1^a	91.24(12)
N1–Ni2–N7^a	90.72(8)	N7–Ni2–N7^a	180.00
N1–Ni2–N1^b	178.56(12)	N1–Ni2–N1^c	88.77(12)
N3–Fe1–N6	89.4(2)	N3–Fe1–C1	93.8(3)
N3–Fe1–C2	179.2(5)	N6–Fe1–C2	91.2(3)
N6–Fe1–C1	92.3(2)	C1–Fe1–C1^d	84.7(2)
N6–Fe1–N6^d	90.52(18)	C1–Fe1–N6^d	175.8(2)
C1–Fe1–C2	85.6(3)		

Symmetry codes: a = -x,1-y,z. b = x,1-y,1/2-z. c = -x,y,1/2-z. d = x,y,-z.

Table S2 Selected bond lengths (Å) and bond angles (°) for **2**.

Fe1-N1	2.166(3)	Fe1-N7	2.198(3)
Fe2-N3	2.016(3)	Fe2-N6	1.995(5)
Fe2-C1	1.926(3)	Fe2-C2	1.947(5)
N1-Fe1-N7	91.0(2)	N1-Fe1-N1^a	91.41(10)
N1-Fe1-N1^b	178.23(10)	N1-Fe1-N7^b	87.2(2)
N1-Fe1-N1^c	88.62(10)	N7-Fe1-N7^a	177.1(3)
N1-Fe1-N7^c	90.8(2)	N7-Fe1-N7^c	177.5(3)
N3-Fe2-C1	92.81(12)	N3-Fe2-N6	88.92(12)
N3-Fe2-C2	90.13(14)	N3-Fe2-N3^d	90.35(12)
N3-Fe2-C1^d	175.71(13)	C1-Fe2-C2	86.96(15)
N6-Fe2-C1	94.05(13)	N6-Fe2-C2	178.6(2)
C1-Fe2-C1^d	83.90(13)		

Symmetry codes: a = 1-x,1-y,z. b = x,1-y,1/2-z. c = 1-x,y,1/2-z. d = x,y,1-z.

Complex	D–H⋯A	H⋯A(Å)	D⋯A(Å)	D–H⋯A(°)
1	O1–H1A⋯N8	2.13	2.83(2)	143
	O1W–H1WA⋯N8	1.78	2.44(2)	132
	O1W–H1WB⋯N2	2.37	2.95(2)	126
	O2W–H2WA⋯O1W	1.63	2.44(3)	159'
	O2W–H2WB⋯O1W	2.55	3.27(3)	144
	C16–H16⋯O1W	2.59	3.41(2)	148
	C18–H18⋯N8	1.77	2.46(2)	129
2	O1–H1A⋯N8	2.30	2.997(19)	143
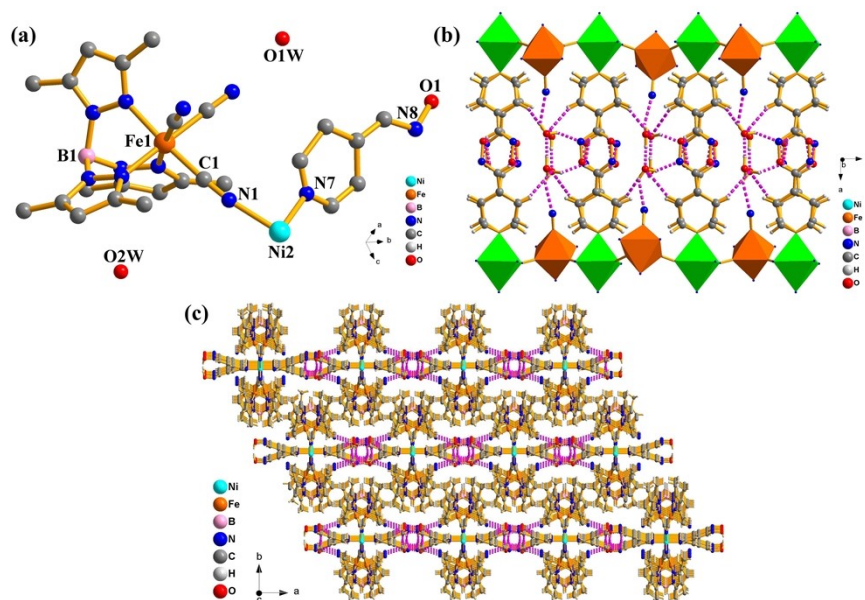
Fig. S1 (a) Perspective view of the asymmetric unit of **1**. (b) A two-dimensional layer through hydrogen bonds along the *ac* plane in **1**. (c) The packing diagram of **1**.
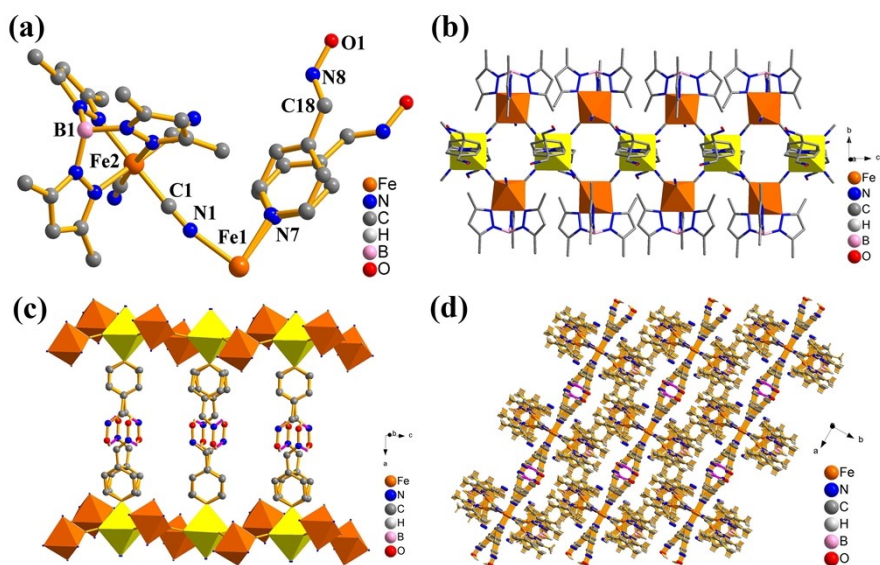
Fig. S2 (a) Perspective view of the asymmetric unit of **2**. (b) One-dimensional (1D) chains formed by cyanide-bridged along the *c* axis for **2**. (c) A two-dimensional layer through hydrogen bonds along the *ac* plane in **2**. (d) The packing diagram of **2**.
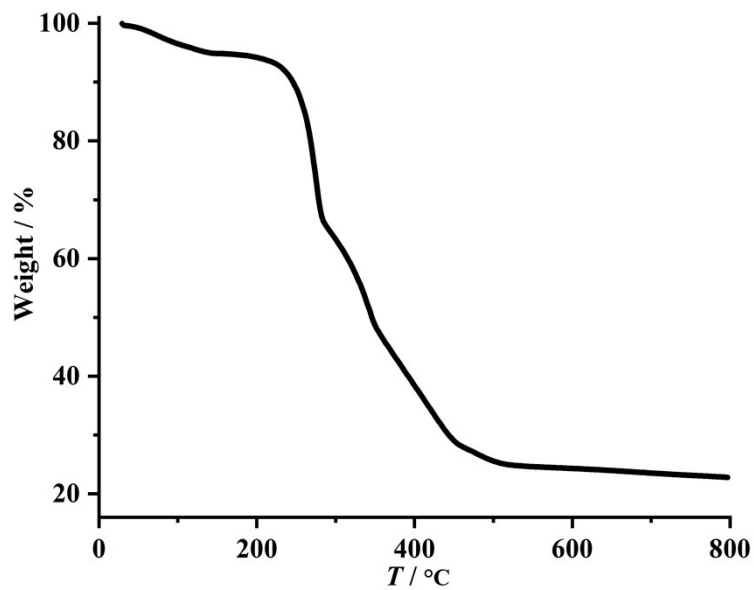
III. PXRD and Thermogravimetric analysis (TGA)
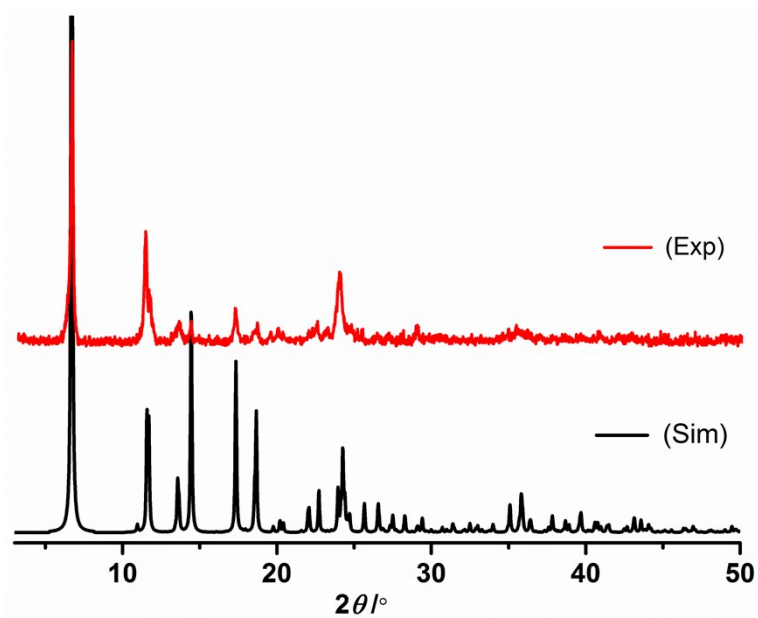
(a)
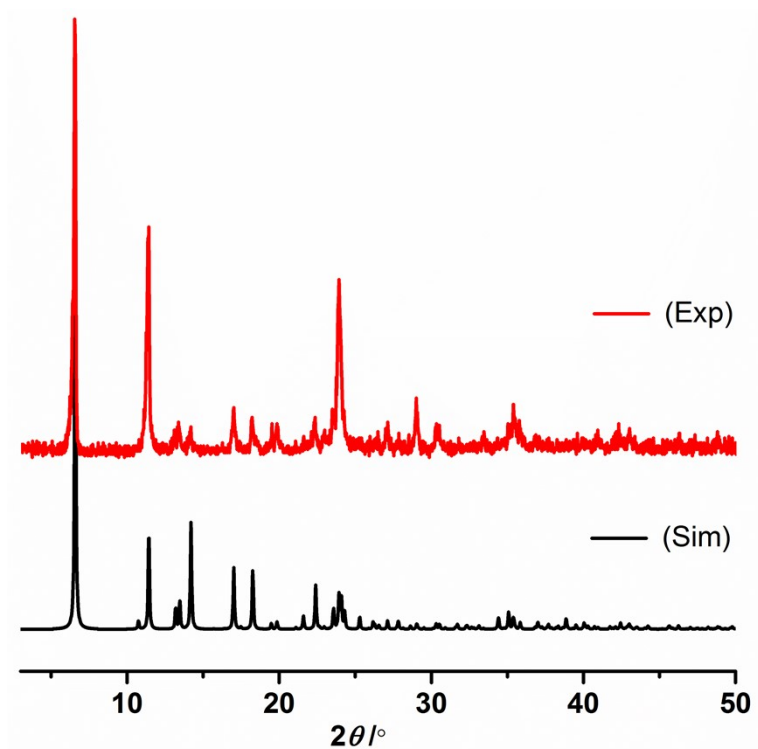
(b)

Fig. S3 Simulated (Sim.) and experimental (Exp.) powder X-ray diffraction (PXRD) patterns for **1** (a), **2** (b).
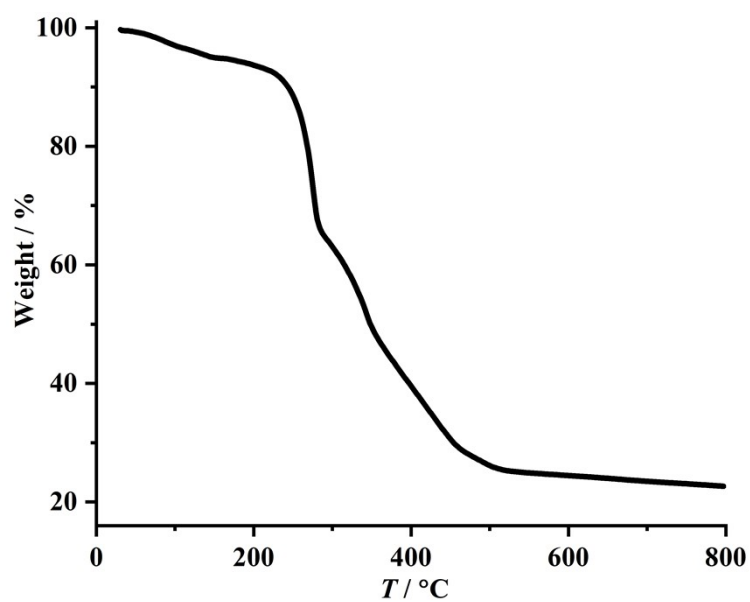
(a)

(b)

Fig. S4 TGA curve for **1** (a), **2** (b).

IV. Magnetic properties
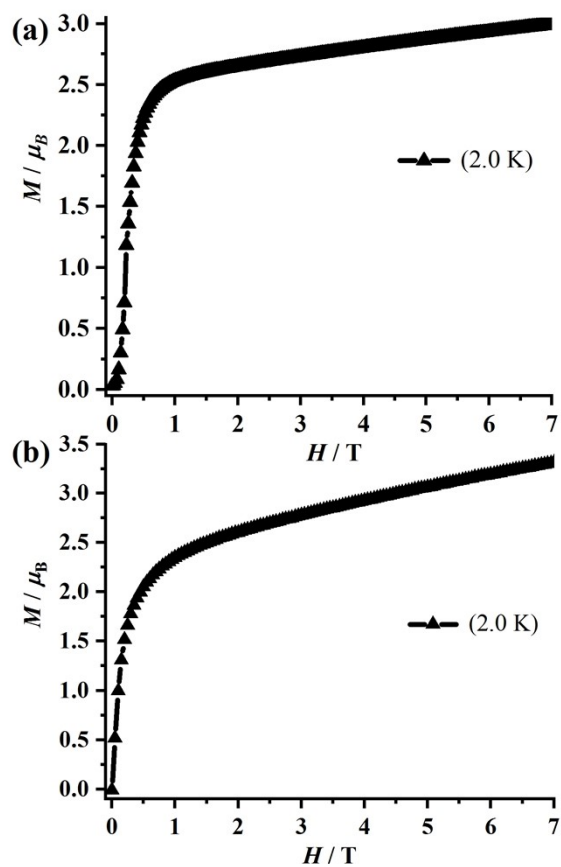
Fig. S5 Magnetization M (μ_B) plotted versus external magnetic field H (T) plot for **1**
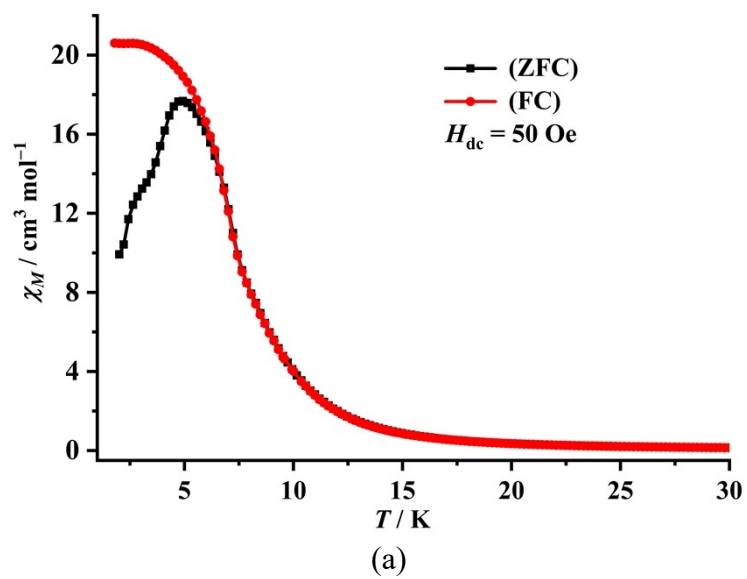
(a) and **2** (b), respectively.
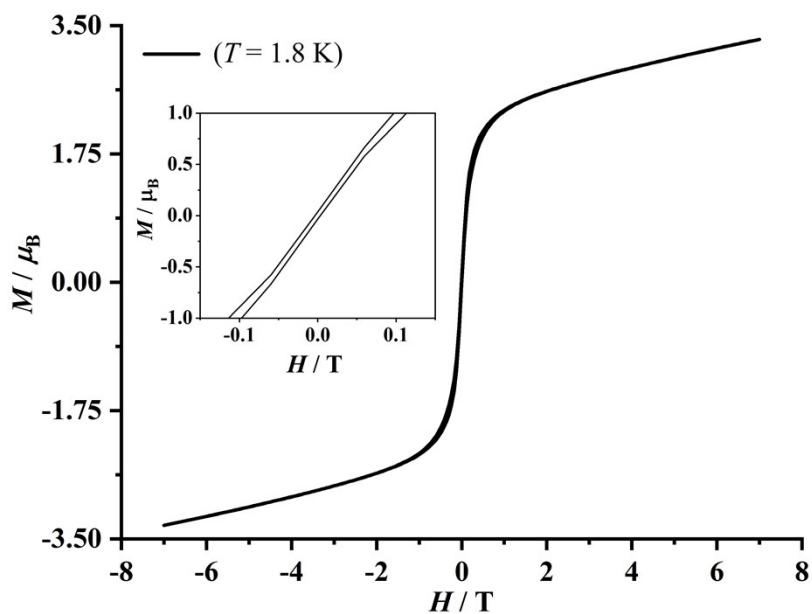
Fig. S6 The magnetic hysteresis loop of **2** recorded at 1.8 K..

(a)
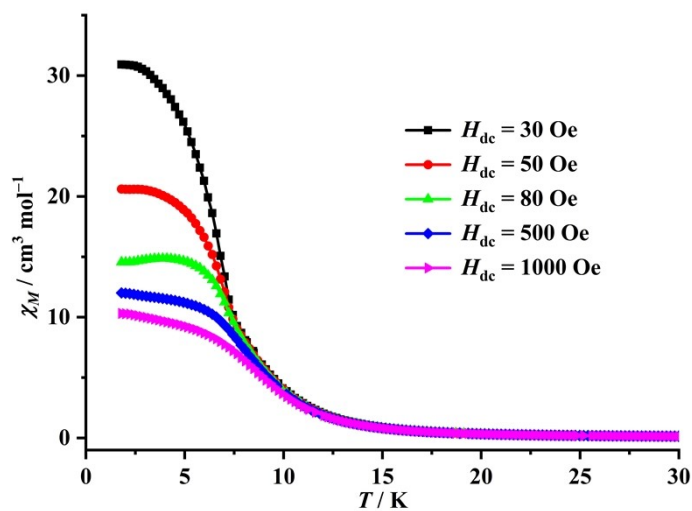
(b)

Fig. S7 (a) ZFC/FC magnetization curves for **1** at an applied field of 50 Oe. (b) FC magnetization curves at various magnetic fields for **1**.
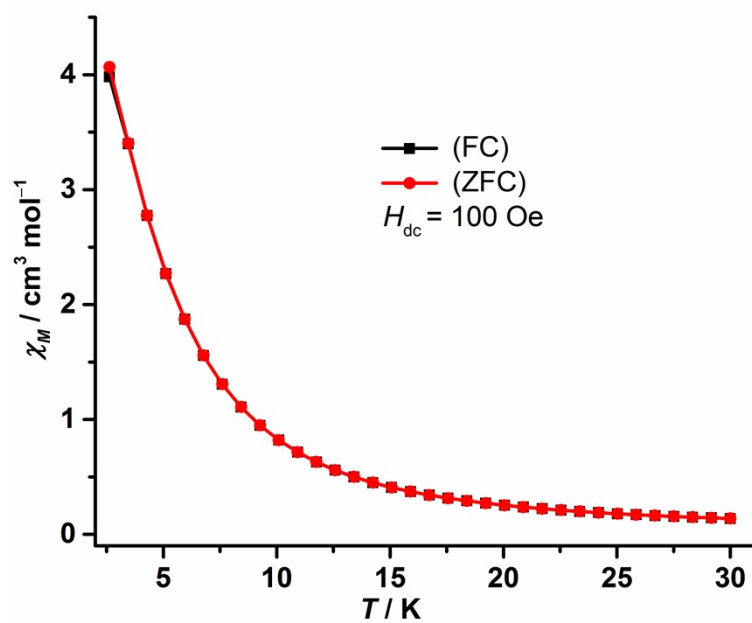

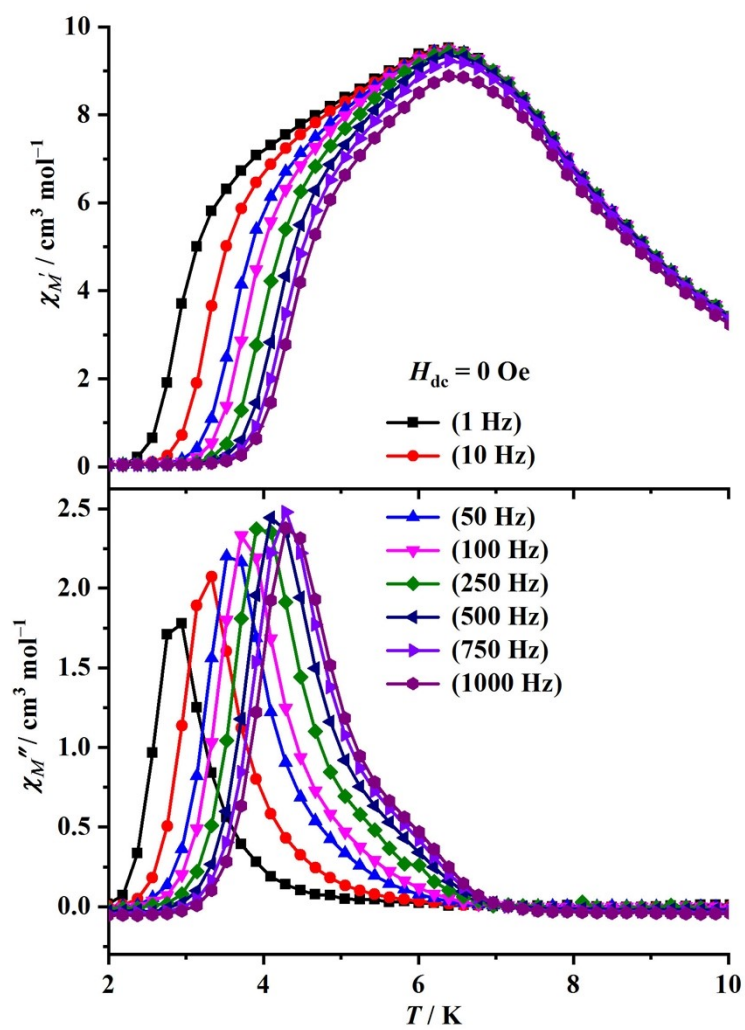**Fig. S8** ZFC/FC magnetization curves at 100 Oe for **2**.

Fig. S9 Temperature dependences of χ' and χ'' for **1** in a 0 Oe DC field in the 1−1000 Hz frequency range.
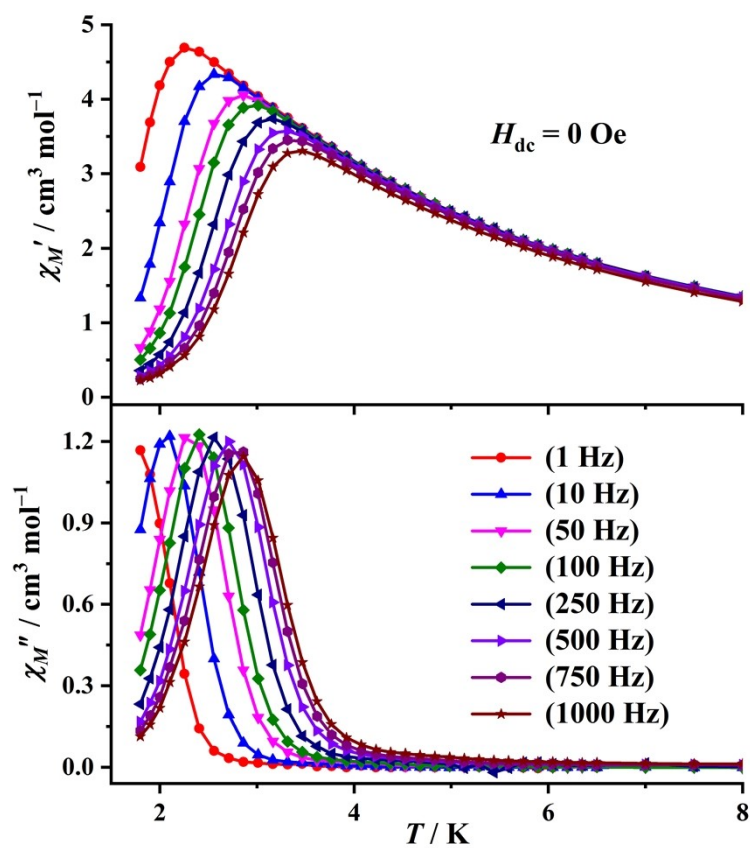
Fig. S10 Temperature dependences of χ' and χ'' for **2** in a 0 Oe DC field in the 1−1000 Hz frequency range.
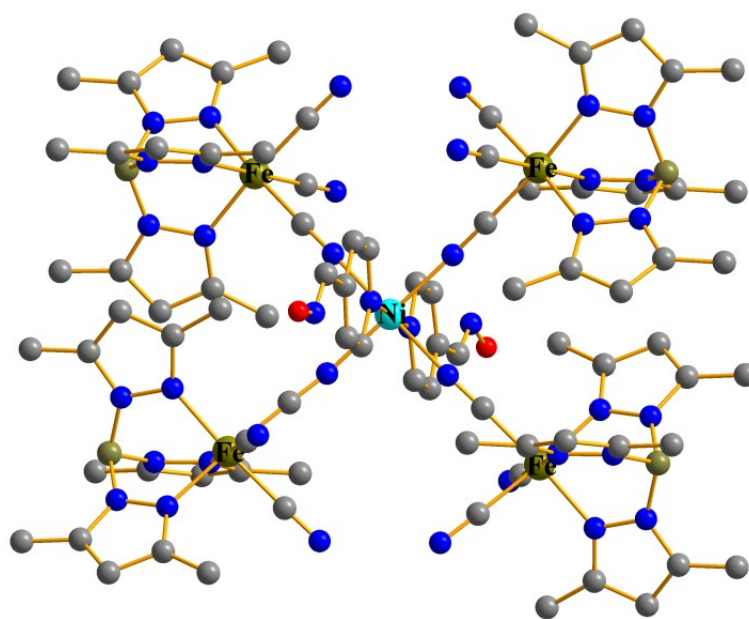
V. Theoretical calculations

Fig. S11 Model structure extracted from complex **1** for calculating Ni^{II}-Fe^{III} exchange

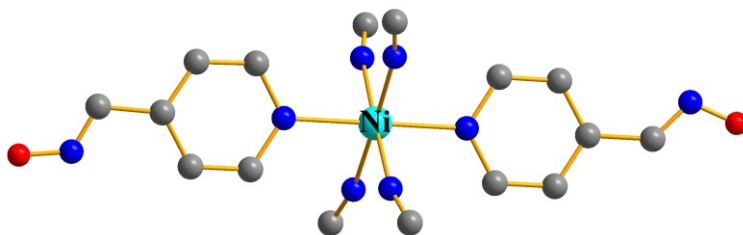interactions; H atoms are omitted for clarity.

Fig. S12 Model structure of individual Ni^{II} fragment.

Table S3. Calculated zero-field splitting parameters $D(E)$ (cm^{-1}) and g (g_x, g_y, g_z) tensors of the lowest spin-orbit state of individual Ni^{II} fragment from complex 1 by CASPT2/RASSI-SO.

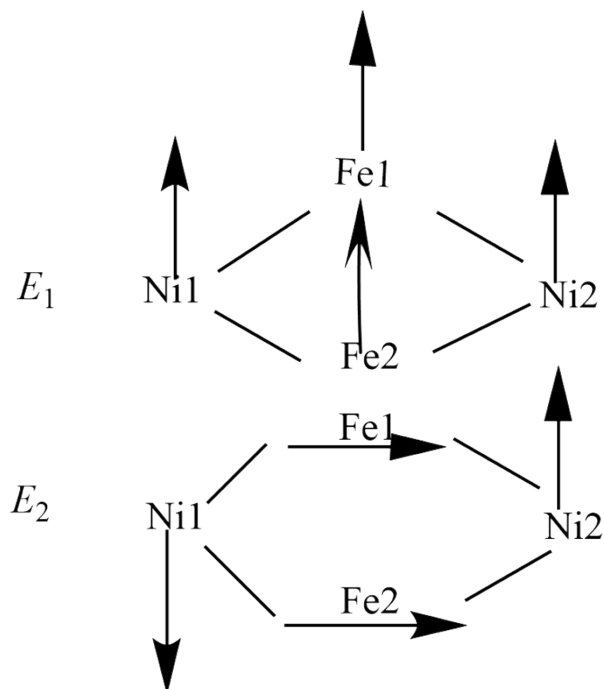| D (E) (cm^{-1})	g
	2.215
−1.41 (−0.44)	2.221
	2.227

Fig. S13 Two spin states of E_1 and E_2.

VI. References

[1] (a) D. Li, S. Parkin, G. Wang, G. T. Yee, A. V. Prosvirin and S. M. Holmes, *Inorg. Chem.*, **2005**, *44,* 4903-4905; (b) M. Nihei, Y. Sekine, N. Suganami, K. Nakazawa, A. Nakao, H. Nakao, Y. Murakami and H. Oshio, *J. Am. Chem. Soc.*, **2011**, *133,* 3592-3600.

[2] G. M. Sheldrick, *Acta Cryst.* **2008**, A*64,* 112-122.

[3] A. L. Spek, *J. Appl. Cryst.* **2003**, *36,* 7-13.

[4] K. Ridier, A. Mondal, C. Boilleau, O. Cador and a. Gillon, *Angew. Chem. Int. Ed.,* **2016**, *55,* 3963

[5] F. Neese, *ORCA–an ab initio, density functional and semiempirical program package, version 4.1.2; Max-Planck institute for bioinorganic chemistry: Mülheim an der Ruhr*, Germany, 2019.

[6] (a) A. D. Becke, *J. Chern. Phys.*, **1993**, *98,* 5648-5652; (b) A. D. Becke, *Phys. Rev. A*, **1988**, *38,* 3098-3100.

[7] C. Lee, W. Yang and R. G. Parr, *Phys. Rev. B*, **1988**, *37,* 785-789.

[8] (a) A. Schäfer, H. Horn and R. Ahlrichs, *J. Chern. Phys.*, **1992**, *97,* 2571-2577; (b) A. Schäfer, C. Huber and R. Ahlrichs, *J. Chern. Phys.*, **1994**, *100,* 5829-5835.

[9] F. Aquilante, J. Autschbach, R. K. Carlson, L. F. Chibotaru, M. G. Delcey, L. De Vico, I. Fdez. Galván, N. Ferré, L. M. Frutos, L. Gagliardi, M. Garavelli, A. Giussani, C. E. Hoyer, G. Li Manni, H. Lischka, D. Ma, P. Å. Malmqvist, T. Müller, A. Nenov, M. Olivucci, T. B. Pedersen, D. Peng, F. Plasser, B. Pritchard, M. Reiher, I. Rivalta, I. Schapiro, J. Segarra-Martí, M. Stenrup, D. G. Truhlar, L. Ungur, A. Valentini, S. Vancoillie, V. Veryazov, V. P. Vysotskiy, O. Weingart, F. Zapata and R. Lindh, *J. Comput. Chem.*, **2016**, *37,* 506-541.